THE JOURNAL OF PHYSICAL CHEMISTRY Letters

Perspective

pubs.acs.org/JPCL

All-Oxide Photovoltaics

Sven Rühle,* Assaf Y. Anderson, Hannah-Noa Barad, Benjamin Kupfer, Yaniv Bouhadana, Eli Rosh-Hodesh, and Arie Zaban*

Department of Chemistry, Bar Ilan University, Ramat Gan 52900, Israel

ABSTRACT: Recently, a new field in photovoltaics (PV) has emerged, focusing on solar cells that are entirely based on metal oxide semiconductors. The all-oxide PV approach is very attractive due to the chemical stability, nontoxicity, and abundance of many metal oxides that potentially allow manufacturing under ambient conditions. Already today, metal oxides (MOs) are widely used as components in PV cells such as transparent conducting front electrodes or electron-transport layers, while only very few MOs have been used as light absorbers. In this Perspective, we review recent developments of all-oxide PV systems, which until today were mostly based on Cu_2O as an absorber. Furthermore, ferroelectric $BiFeO_3$-based PV systems are discussed, which have recently attracted considerable attention. The performance of all-oxide PV cells is discussed in terms of general PV principles, and directions for progress are proposed, pointing toward the development of novel metal oxide semiconductors using combinatorial methods.

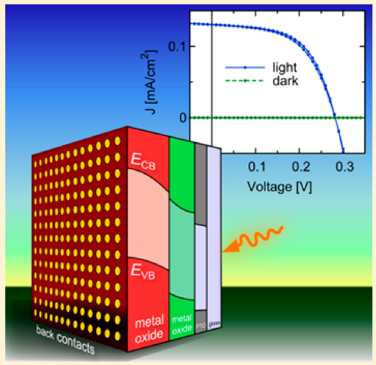

The market for photovoltaic (PV) modules has shown nearly exponential growth over the last years, with a peak power of more than 25 GW installed in 2011, leading to a cumulative installed capacity of ~70 GW.[1,2] For comparison, a typical nuclear power plant can produce around 1 GW. Even though the PV sector is booming, PV-generated electricity in most places can still not compete in price with conventionally generated electricity and is consequently dependent on subsidies.[3] To reach grid parity, further price reductions for PV systems are required, calling for continued up-scaling of the production processes or for novel PV cell concepts based on cheap materials and low-cost deposition methods. Metal oxide (MO) semiconductors are very attractive to achieve that goal; they are chemically stable, and many MOs are nontoxic, abundant, and fulfill the requirements for low-cost manufacturing methods at ambient conditions. Consequently, devices made of MO semiconductors can be very inexpensive, stable, and environmentally safe, which are, besides the conversion efficiency, the most important requirements for PVs. From the optical point of view, there are a number of MOs suitable for PV applications. However, the electronic properties of most known MOs, that is, the short lifetime of excited electronic states and low mobility of electronic charge carriers, prevented their use as active solar cell materials. Here, we give a perspective on all-oxide PVs as a future technology for economic energy generation. We show where MOs are today applied as components in PV cells, review existing all-oxide PV systems, and discuss their limitations. Combinatorial methods are proposed for synthesis of novel multicomponent MOs, including doped oxides, new crystalline or amorphous MOs, and MO composites, which can overcome the current limitations.

Metal Oxides in PVs. MOs are today widely used as components in PV cells and modules, mainly as transparent conducting oxides (TCOs).[4,5] Fluorine-doped tin oxide (FTO), indium tin oxide (ITO), or aluminum-doped zinc oxide (AZO) are the most common TCOs and widely applied in commercially available thin film solar cells based on CdTe, $CuIn_xGa_{1-x}Se_2$ (CIGS), and amorphous or microcrystalline Si, which have a market share altogether of around 17%.[1] Besides PV, TCOs are used in consumer electronics for flat panel displays, touch screens, and smart phones. Very dynamic research is reported from the field of thin film transistors based on wide-band-gap MOs, which are very attractive due to the optical transparency that is added to the electronic functionality.[6]

> Recently, a new field in photovoltaics has emerged, focusing on solar cells that are entirely based on metal oxide semiconductors.

Promising next-generation nanocomposite PV cells such as dye-sensitized solar cells (DSCs),[7] quantum-dot-sensitized solar cells (QDSCs),[8] or extreme thin absorber cells (ETA cells)[9] are based on nanostructured MO electrodes that are deposited onto a TCO substrate and are coated with a thin absorber layer from which charge carriers (in most cases, electrons) are injected into the MO upon photoexcitation.[10,11] Nanostructured electrodes based on TiO_2,[12] ZnO,[13] SnO_2,[14] $SrTiO_3$,[15] Nb_2O_5,[16] and ZrO_2[17] have been used as wide-band-gap electron conductors, while NiO has been used as a hole-transport material.[18] Light to electric power conversion efficiencies of 11−12% have been achieved with DSCs where

Received: October 22, 2012
Accepted: November 30, 2012
Published: December 5, 2012

   dx.doi.org/10.1021/jz3017039 | *J. Phys. Chem. Lett.* 2012, 3, 3755−3764

a mesoporous TiO_2 film was used as an electron conductor with a high microscopic surface area for dye adsorption.[19,20] Recently, mesoporous Al_2O_3 was used as a high-surface-area matrix to accommodate an organometallic halide perovskite absorber and spiro-OMeTAD as a hole conductor. In contrast to the common DSC, QDSC, or ETA cell concepts, no charges were injected into the mesoporous Al_2O_3, leading to solar cells with an efficiency above 10% due to efficient electron transport along the absorber coating.[21] MO electrodes can be produced in a variety of nanostructures such as mesoporous films,[22] nanorods,[23] nanowires,[24] nanotubes,[25] and more complex morphologies,[26,27] with ZnO being the most versatile material in terms of growth conditions and shapes.[28] For polymer-based PV cells, MOs such as TiO_2 and ZnO have been used as electron acceptors in flat[29] as well as nanostructured devices.[30−32] As hole-transport materials, NiO,[33] V_2O_5,[34] WO_3,[35] and MoO_3[36] have been used in organic solar cells.[37,38]

Metal oxide semiconductors are very attractive; they are chemically stable, and many oxides are nontoxic, abundant, and fulfill the requirements for low-cost manufacturing at ambient conditions.

Cu_2O-Based All-Oxide PVs. In this Perspective, we present a comprehensive view of all-oxide PV, from which one can gain better understanding of the system and point out directions for progress. Only a few MOs have been investigated as light absorbers for PV applications where Cu_2O is the most popular material (see Table 1), with extensive research going back to the 1970s.[64,65] As a single-junction device, its electronic band gap of approximately 2.0 eV is not ideal for the sun spectrum (AM1.5G), leading to a maximum theoretical conversion efficiency of ∼23% compared to 32.9% for an optimized band gap of 1.34 eV (detailed balance limit).[66] However, as a top cell in a multijunction stack consisting of three or more junctions, its band gap is nearly optimized;[67] furthermore, Cu_2O can be a very attractive absorber for semitransparent PV cells.

Table 1. Reported All-Oxide PV Cells

absorber	junction	interface type	refs
Cu_2O	Me/Cu_2O	Schottky junction	39−41
Cu_2O	ZnO/Cu_2O	bilayer heterojunction	42−47
Cu_2O	*n*-Cu_2O/*p*-Cu_2O	bilayer homojunction	48−51
CuO/Cu_2O	CuO/Cu_2O	bilayer heterojunction/electrolyte contact	52
Cu_2O	nanowire ZnO/Cu_2O	nanocomposite heterojunction	53−57
Cu_2O	mesoporous TiO_2/Cu_2O	nanocomposite heterojunction	58
Cu_2O	nanotube TiO_2/Cu_2O	nanocomposite heterojunction	59
$BiFeO_3$	$BiFeO_3$ domain boundaries	ferroelectric domain boundaries	60−63

Cu_2O can be produced by a number of methods, including high- and low-temperature thermal oxidation,[68] electrochemical deposition,[69] anodic oxidation,[70] spray pyrolysis,[71] and reactive sputtering[72], and is mostly p-type. Initial PV device structures were based on a Schottky junction, where it was found that the photovoltage did not scale with the work function difference between the Cu_2O and the metal contact, which was attributed to a Cu-rich phase that is formed in the vicinity of the contact (schematically shown in Figure 1a).[41] The open-circuit voltage

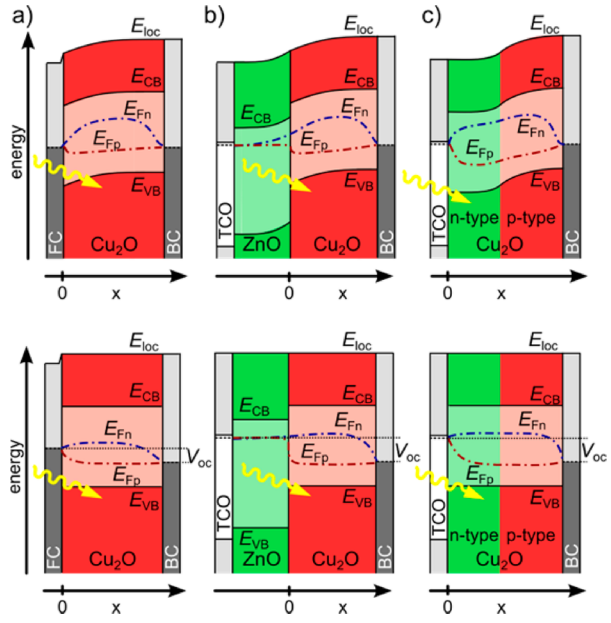

Figure 1. Schematic energy band diagrams of Cu_2O-based all-oxide PV cells at short circuit (top) and open circuit (bottom), showing the local vacuum level (E_{loc}) and the valence and conduction band edge (E_{VB} and E_{CB}, respectively). The gradients of the hole and electron quasi-Fermi levels (E_{Fn} and E_{Fp}) at open circuit indicate that substantial recombination occurs at the front and back contacts (FC and BC). (a) Cu_2O Schottky junction, illuminated through a TCO or thin metal FC. (b) ZnO/Cu_2O heterojunction cell illuminated through the TCO and ZnO window layer. (c) A n−p Cu_2O homojunction solar cell shown with illumination from the n-type side; however, also backside illumination has been reported when a TCO is used as a BC.

(V_{oc}) of the resulting Cu/Cu_2O Schottky junction solar cell was below 0.6 V;[39,40] however, photovoltages above 1 V are required to achieve light to electric power conversion efficiencies above 10% with a Cu_2O absorber. Consequently, heterojunction devices were developed, mainly with ZnO as an intrinsic n-type semiconductor and Cu_2O as the p-type absorber, produced by electrodeposition,[43,44] sputtering,[42] or thermal oxidation of Cu foil.[45] Though a similar Cu enrichment was also found in ZnO/Cu_2O heterojunction solar cells,[42] record light to electric power conversion efficiencies of around 4% were achieved.[46,47]

Besides ZnO, other MOs have been used to form bilayer heterojunction all-oxide solar cells such as CuO/Cu_2O[52] and CdO/Cu_2O,[73] where in the latter case, the measured currents and voltages were so low that it was not clear if this heterojunction showed real PV activity. The reported synthesis of n-type Cu_2O[74] triggered the fabrication of Cu_2O-based n−p homojunction solar cells,[48−51] though the origin for the n-type doping is under debate.[75]

For Cu_2O, it was argued that the inverse absorption coefficient α^{-1} is larger than the minority carrier diffusion length L_D, causing substantial recombination within the light absorber. Nanostructured interfaces have been proposed to improve charge separation (Figure 2), and ZnO nanowires were used in Cu_2O absorber PV cells. It was shown that the

dx.doi.org/10.1021/jz3017039 | J. Phys. Chem. Lett. 2012, 3, 3755−3764

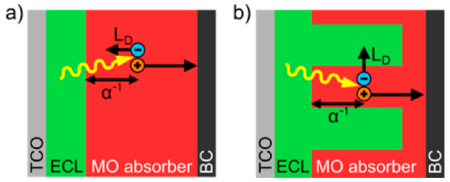

Figure 2. (a) Schematic drawing of a thin film all-oxide PV cell consisting of a TCO FC, a wide-band-gap electron-conducting layer (ECL), a MO absorber, and a metal BC. Significant losses occur because the electron diffusion length L_D is shorter than the penetration depth α^{-1} of the light. (b) Nanostructured interfaces can be used to decouple both length scales, providing an interface for charge separation within L_D while α^{-1} is still larger than L_D.

short-circuit current density (J_{sc}) was increased compared to that for a flat bilayer reference solar cell,[54] but the conversion efficiency remained below 1%,[53,55−57] thus significantly below the performance of the good bilayer systems. Furthermore, Cu_2O was grown electrochemically within mesoporous TiO_2 films[58] and arrays of TiO_2 nanotubes,[59] but also here, the conversion efficiency remained below 1%.

$BiFeO_3$-Based PVs. PV cells based on ferroelectric oxides such as $BiFeO_3$ have been reported recently.[60−63] Solar cells with a lateral design were presented, where two Pt contact stripes were deposited on top of a $BiFeO_3$ film parallel to the domain boundaries. Even though the device had a symmetric structure, it was explained recently that the required asymmetry to generate a photocurrent and voltage originated from the electric field within the domains and at the domain boundaries.[61] The domains were electrically connected in series while illuminated in parallel with the same light intensity. The band diagram in Figure 3 (top) shows a schematic energy band diagram of the $BiFeO_3$ PV system at short circuit. An electric field in the domain generates a drift current such that photogenerated electrons and holes move toward opposite

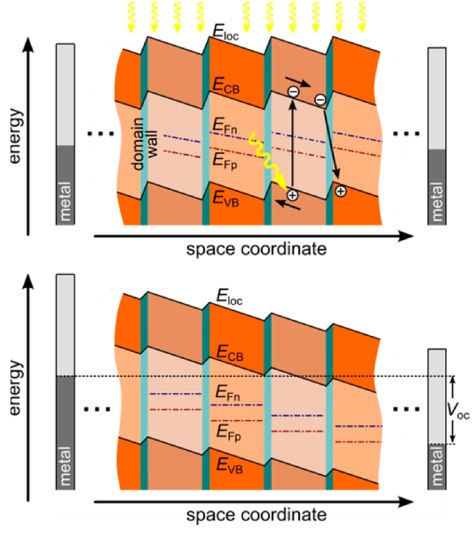

Figure 3. Energy band diagrams for $BiFeO_3$-based solar cells according to ref 63 at short (top) and open circuits (bottom), showing the ferroelectric domains where the width of the domain walls is exaggerated for better visibility. Due to the lateral design, each domain is exposed directly to the light. Electrons and holes migrate toward domain walls where they recombine with carriers from the neighboring domain. At open circuit, high photovoltages are achieved due to the electronic series connection of the domains.

domain boundaries where they recombine with charge carriers of opposite sign from the neighboring ferroelectric domain.[61,63] The maximum photovoltage generated at a single ferroelectric junction was determined to be on order of 10 mV.[63] With tens to hundreds of ferroelectric domains connected in series, photovoltages up to 15 V have been reported, which is schematically shown in Figure 3 (bottom).[63] It was furthermore shown that the direction of the photocurrent was switchable by an electrostatic potential applied before illumination.[60,62] Ferroelectric $BiFeO_3$-based PV cells have recently generated considerable interest; however, it seems unlikely to reach light to electric power conversion efficiencies that are relevant for electricity generation. The intrinsic limitations of $BiFeO_3$ for PV applications will be discussed in more detail below.

PV Principles. To bring the concept of all-oxide PV to a breakthrough, we believe that more MOs have to be investigated for PV applications and new multicomponent MOs have to be developed in conjunction with an optimized device design. This requires an understanding of the working principle of PV cells, and we review in the following the fundamental principles for PV action. To describe PV cells in terms that are applicable to all possible device structures including p−n homo- and heterojunction cells (i.e., Si, CIGS, CdTe, Cu_2O), bulk heterojunction devices (i.e., plastic solar cells), nanostructured photoelectrochemical cells (i.e., DSCs, QDSCs), or ferroelectric domain boundary cells (i.e., $BiFeO_3$), we follow a generalized approach.[76,77]

(i) Any PV device requires a light absorber that converts electrons from thermal equilibrium into an excited state upon absorption of photons (Figure 4a).

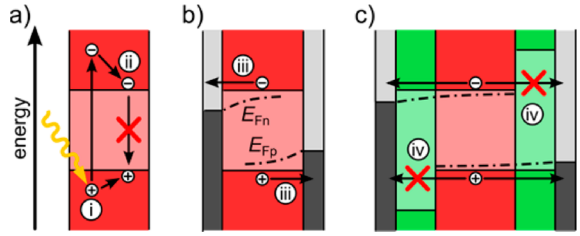

Figure 4. General principle of PVs. (a) Upon photon absorption, an electron is excited into an electronic state at higher energy, leaving a positive charge behind at low energy (process i). These charges are transferred into a metastable high- and low-energy state (process ii). (b) A driving force is required (shown by a gradient in the quasi-Fermi levels E_{Fn}, E_{Fp}) to transport the electron to an external contact at high electron energy while the positive charge has to reach the "low-energy contact" (process iii). (c) Furthermore, the contacts have to be selective to one type of charge carrier, preventing positive and negative charges from reaching the oppositely charged contact (process iv).

(ii) Either this excited state is metastable by itself or the electron is transferred into a metastable, high-energy state while the remaining positive charge gets into a metastable low-energy state (Figure 4a).

(iii) A transport mechanism is required to bring electrons to a "high electron energy contact (negative potential)", while the remaining positive charge needs a driving force to get to a "low-energy contact" (Figure 4b).[76]

(iv) The contacts have to show some selectivity for charge collection such that positive charges cannot recombine with electrons from the high-energy contact, while electrons from the high energy-state should not reach the low-energy contact (Figure 4c).

dx.doi.org/10.1021/jz3017039 | J. Phys. Chem. Lett. 2012, 3, 3755−3764

This rather abstract definition describes all types of PV cells, which can be easily applied to cells with an intrinsic absorber (n−i−p or p−i−n). Electrons are excited into some electronic state in the conduction band, directly followed by phonon emission such that electrons decay to the bottom of the CB, which is the metastable high-energy state. The electric field across the intrinsic layer provides a driving force for electron and hole transport toward the respective contact, while a doped n- and p-type layer close to the high- and low-energy contact provides the required transport selectivity due to a VB offset that creates a barrier for hole transport toward the FC, and a CB offset between the absorber and the p-type layers blocks electrons from recombining at the BC.[78] Plastic solar cells operate very similar to p−i−n cells with the difference that the metastable high-energy state corresponds to the LUMO level of the acceptor while the HOMO level of the donor defines the low-energy state. PV action in p−n homojunction Si cells is often entirely attributed to the built-in electric field that provides a driving force for holes and electrons toward the FC and BC, respectively. However, selective charge collection at the FC is at least as important to achieve high conversion efficiencies.

While the above principles are basic requirements for PV action, they do not say much about the efficiency of the process. For the development of efficient single-junction PV cells, additional criteria have to be fulfilled.

(v) The band gap of the absorber should be in the range between 0.9 and 1.7 eV (absorption onset between 1380 and 730 nm), for which the detailed balance limit predicts a theoretical efficiency limit above 30%.

(vi) The inverse absorption coefficient α^{-1} should be shorter than the minority carrier diffusion length L_D.

(vii) During the transport from the absorber to the high- and low-energy contact, the loss of energy due to discontinuities of the valence or the conduction band have to be minimized.

Criteria (v) is a result of detailed balance calculations that take into account that photons with sub-band-gap energy are not absorbed ($h\nu < E_g$) while only a fraction of the photon energy ($E_g/h\nu$) above the band gap is converted into electric power while the fraction $(h\nu - E_g)/h\nu$ is mostly converted into heat. Criteria (vi) is a rather rough statement saying that within a minority carrier diffusion length, most of the photons should be absorbed in order to provide diffusion as a transport mechanism to reach the respective contact. This statement is useful for the development of new absorber materials because α^{-1} as well as L_D are material properties and can be characterized without the need to produce a complete solar cell. However, criteria (vi) neglects additional parameters that can cause a gradient of the minority carrier quasi-Fermi level (which is the driving force minority carrier), such as the electric fields, gradients of the electron affinity, and band gap or band discontinuities. In contrast to the diffusion length, these parameters are defined by the device structure and can only be characterized in a complete solar cell. The same applies for criteria (vii), which provides a general guideline for the band structure of a solar cell. Figure 5 shows the energy band diagram of a nonideal and an optimized n−p heterojunction cell at short and open circuit including interface dipoles (ΔE_{loc}) causing changes of E_{loc} on very short length scales, conduction band discontinuities (ΔE_{CB}) at interfaces due to differences in the electron affinities of the junction materials, and interface dipoles, while valence band discontinuities (ΔE_{VB}) contain additionally the difference in the band gap of the junction-forming materials. Figure 5 shows that higher photovoltages can be achieved when ΔE_{CB} is minimized at each interface between the absorber and the high-energy contact (in the depicted case, the FC), while ΔE_{VB} has to be minimized between the absorber and BC. Conceptually, interface dipoles can compensate for band edge offsets, but it requires major efforts to find materials that show the desired electronic properties and can be deposited in the thickness of a few monolayers in between two junction-forming semiconductors.

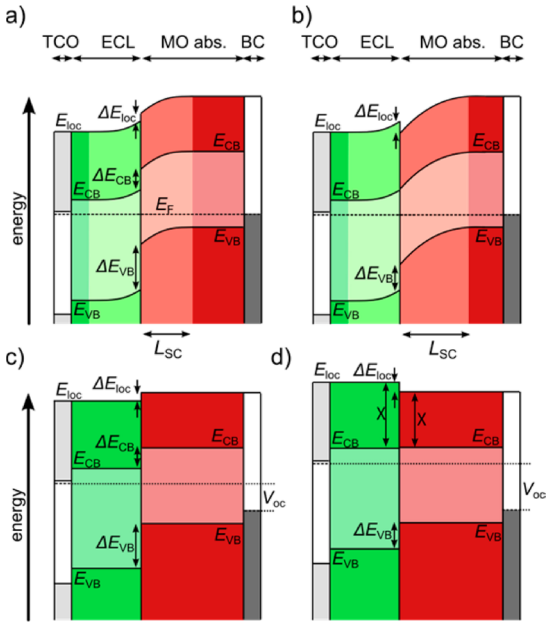

Figure 5. Nonoptimized and optimized n−p heterojunction solar cells consisting of a TCO front electrode, an ECL, a MO absorber, and a BC, shown in the dark (top) and at open-circuit potential (bottom). (a) Nonoptimized band structure with losses due to a CB offset ΔE_{CB} at the heterojunction. (b) Optimized system showing an interface dipole (ΔE_{loc}) that compensates for the difference of electron affinity (χ) of the ECL and MO absorber. (c) Under illumination, the nonoptmized device reaches a lower open-circuit voltage V_{oc} compared to the optimized structure (d).

Discussing the all-oxide PV concepts reviewed above in terms of principles for efficient solar cell operation reveals the weaknesses of existing systems. The generation intensity of electron−hole pairs is derived from Beer−Lambert law, $G(x) = G_0 \exp(-\alpha x)$, where G_0 is the generation intensity in the absorber at the site of incident light ($x = 0$). Thus, most of the electron−hole pairs are generated close to the FC, and the electric field at the Schottky junction is the only driving force that provides some selectivity to the FC, that is, preventing holes from reaching the contact. Under the applied bias, this Schottky barrier is reduced, and recombination at the FC increases (Figure 1a bottom), leading to a low fill factor and photovoltage. Introducing a window layer such as ZnO between the FC and the Cu_2O can efficiently block holes from reaching the front electrode due to a valence band offset at the ZnO/Cu_2O interface that creates a barrier for hole transport. Experimentally, this was verified by Mittiga et al., who showed that an ITO/ZnO/Cu_2O/Cu heterojunction solar cell performs significantly better compared to an ITO/Cu_2O/Cu solar cell, which is similar to a Schottky junction cell with ITO as a front electrode instead of a thin semitransparent metal layer.[45] The device including the ZnO window layer reached a higher I_{sc}, V_{oc}, fill factor, and efficiency (~2%) compared to the

dx.doi.org/10.1021/jz3017039 | J. Phys. Chem. Lett. 2012, 3, 3755−3764

Schottky-type device. The highest conversion efficiencies of around 4% reported today are all based on devices that employ an intrinsic n-type ZnO window layer between the TCO and the Cu_2O using AZO as a TCO. This might lead to an improved band diagram with lower energy losses when photoexcited electrons are transported from the Cu_2O CB to the FC.[46,47] Furthermore, thermal oxidation of pure Cu sheets (≥99.9%) is commonly used to achieve polycrystalline Cu_2O with large single-crystalline grains on the order of tens of mm^2, thus reducing recombination at grain boundaries and impurity states, which finally leads to such promising conversion efficiencies.

Cu_2O n−p homojunction cells as proposed by McShane et al.[49] or Wei et al.[51] were produced without a window layer between the TCO and the Cu_2O, thus providing a recombination path via the FC, next to the place of the highest-generation intensity of electron−hole pairs. The V_{oc} and fill factor remained very low (on the order of 100 mV and 25%, respectively) when such cells were illuminated from the side of the n-type Cu_2O that was deposited onto commercial FTO,[51] while better a V_{oc}, I_{sc}, and fill factor were achieved when the n-type Cu_2O was illuminated via an ITO BC that was deposited by sputtering.[49] This example shows that the choice of TCO and deposition method strongly affects the interface properties and subsequently the cell performance. Deuermeier et al., for example, showed that the VB offset at ITO/Cu_2O interfaces, where both materials were prepared by reactive magnetron sputtering, can differ by up to 0.5 eV depending on the deposition conditions such as sample heating.[72]

In $BiFeO_3$ PV cells, electrons and holes are separated by the ferroelectric field in a single domain, which provides some selectivity of charge collection at the contact or, better, at the domain wall. An intrinsic limitation of $BiFeO_3$ for PV application is its rather wide band gap of ∼2.7 eV in conjunction with the low photovoltage generated at a ferroelectric domain boundary. If a photon with an energy of 2.7 eV excites an electron−hole pair that can generate a photovoltage on the order of tens of mV, say, for example, 27 mV, then 99% of the photon energy is not converted into electric energy even if the quantum efficiency for such a process is 100%. Considering furthermore that most of the photons from the sun have an energy below the band gap of 2.7 eV, it becomes clear that $BiFeO_3$ cells in their current form will not play a role for energy generation, even though they are a highly interesting system from a scientific point of view.

New All-Oxide Heterojunction PV Cells. To bring all-oxide PV to a breakthrough, we believe that new materials have to be investigated. We have recently developed new all-oxide bilayer heterojunction cells using CuO and Co_3O_4 as light absorbers, which have a more suitable band gap for the sun spectrum compared to Cu_2O in order to achieve high light to electric power conversion efficiencies. Furthermore, we investigated Fe_2O_3 as a light absorber, which is attractive due to its abundance and chemical stability. The CuO- and Co_3O_4-based PV cells consisted of a FTO FC onto which a compact TiO_2 layer was deposited by spray pyrolysis,[79] followed by pulsed laser deposition (PLD) of the CuO or Co_3O_4 absorber. For the BC, a 10 nm thin Cr layer was sputtered to achieve good adhesion to the absorber followed by a 80 nm thick Au layer to guarantee good electric contact to the external measurement circuit.

I−*V* curves measured in the dark and under illumination (simulated AM1.5G spectrum) are shown in Figure 6a,b for bilayer heterojunctions TiO_2/CuO and TiO_2/Co_3O_4. All *I*−*V* curves were recorded in ascending and descending scan direction to exclude hysteresis due to charge trapping and to guarantee quasi-steady-state conditions in each measurement point. Optical transmission and reflection measurements were carried out to determine the band gap of the absorber from $(\alpha h\nu)^n$ versus $h\nu$ plots,[80] with n = 2 for direct band gap semiconductors and n = 1/2 for indirect band gaps, shown on the right-hand side in Figure 6. For the CuO-based cell, an

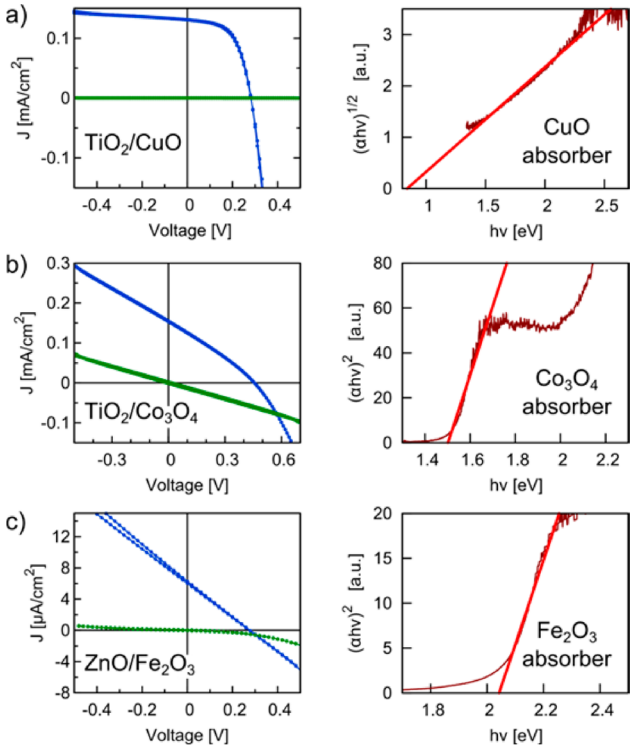

Figure 6. Novel all-oxide PV cells. *I*−*V* characteristics (left) in the dark (green) and under illumination (blue) of novel bilayer heterojunction all-oxide PV cells. On the right-hand side $(\alpha h\nu)^n$ versus $h\nu$ plots are shown from which the band gaps were derived with n = 2 for direct and n = 1/2 .for indirect band gap materials. (a) Cell structure like that in Figure 2a, consisting of a FTO FC, a compact TiO_2 layer, a compact CuO light absorber, and a Cr/Au metal BC. (b) Like (a) with a Co_3O_4 absorber. (c) All-oxide PV cell based on a FTO FC, a compact ZnO layer, a compact Fe_2O_3 light absorber, and a Cr/Au BC.

indirect band gap at around 0.9 eV was derived, which is lower compared to literature values that range from 1.2 to 1.7 eV.[81,82] The *I*−*V* under illumination showed a strong rectifying behavior leading to a high fill factor, but the overall conversion efficiency remained very low due to a short-circuit current density on the order of 100 $\mu A/cm^2$. For the Co_3O_4-based solar cell (Figure 6b), a direct band gap of 1.5 eV was derived from the Tauc plot, which is nearly optimized for a light absorber in a single-junction PV cell. The dark *I*−*V* curve shows a significant slope at around zero voltage, indicating that the cell had a rather low shunt resistance, which is further reduced under illumination (steeper slope). Under illumination, the Co_3O_4-based cell reached a V_{oc} of around 400 mV; however, the J_{sc} remained in the sub-mA/cm^2 regime, and together with the low fill factor, the conversion efficiency stayed far below 1%.

For the Fe_2O_3 heterojunction cell, ZnO was chosen as a window material, and both MOs were produced by PLD. ZnO

dx.doi.org/10.1021/jz3017039 | J. Phys. Chem. Lett. 2012, 3, 3755−3764

has a lower CB edge (further away from the local vacuum level E_{loc}) compared to TiO_2, which is essential to enable electron injection from Fe_2O_3. From the Tauc plot (Figure 6c), an absorption onset at 2.05 eV was derived where, in contrast to literature, Fe_2O_3 was treated as a direct band gap semiconductor because it was not possible to identify a linear region when $(\alpha h\nu)^{1/2}$ was plotted versus $h\nu$. Further optical and structural investigations are underway to clarify the origin of this behavior. $I-V$ measurements clearly showed PV activity, but the photocurrent remained very low, on the order of a few $\mu A/cm^2$. The dark $I-V$ curves of all three all-oxide bilayer heterojunction cells did not show any pronounced rectifying behavior in this potential range, while the light $I-V$ curves display rectification for the CuO- and Co_3O_4-based cells. Furthermore, all three all-oxide PV systems show a crossover of the light with the dark $I-V$ curve, indicating that photoconductivity plays a role in device operation. The results above demonstrate that it is not difficult to find new all-oxide PV heterojunctions with a very low performance. Even for materials with a nearly optimized band gap such as CuO or Co_3O_4, the current densities remained roughly 2 orders of magnitude below their theoretical limit, calling for better materials and an improved device design.

To develop efficient all-oxide PV cells, a combinatorial approach is proposed where a large number of experiments are conducted on a single substrate. This provides a method for fast development of novel materials and optimization of device structures. We distinguish between (a) combinatorial all-oxide PV cells (device libraries) and (b) combinatorial material science (material libraries).

The prospect of finding these unique materials lies in combinatorial material science.

Combinatorial All-Oxide PV Device Libraries. All-oxide PV device libraries suitable for high-throughput characterization to investigate the impact of the individual layer thicknesses in the multilayer stack are presented. This powerful approach was used to investigate the minority carrier diffusion length of CuO in the TiO_2/CuO heterojunction all-oxide PV cell presented in Figure 6a. An entire solar cell device library was created on precut glass substrates (72 × 72 mm^2) covered with FTO (Pilkington, 7 Ω/square) onto which a compact TiO_2 layer with a linear thickness gradient was deposited by spray pyrolysis[79] followed by PLD of CuO without sample rotation to create an inhomogeneous thickness profile (Figure 7). A grid of 13 × 13 metal BCs (Cr/Au) was deposited by sputtering onto the absorber layer using a shadow mask where each contact patch had a diameter of 2.3 mm, corresponding to an area of ~0.04 cm^2 and a minimum spacing of 2.7 mm in between neighboring patches. The sprayed TiO_2 and PLD-deposited absorber layer were mechanically scraped off from the library edges with a diamond pen before a frame of the soldering alloy was deposited by ultrasonic soldering for good electrical contact to the FTO FC, schematically shown in Figure 7b,d. In that way, a library of 169 solar cells was created of varying the MO layer thicknesses, with FTO as a joint FC. The solar cell area was estimated by the size of the BC, neglecting lateral charge collection from areas surrounding the contact patch.

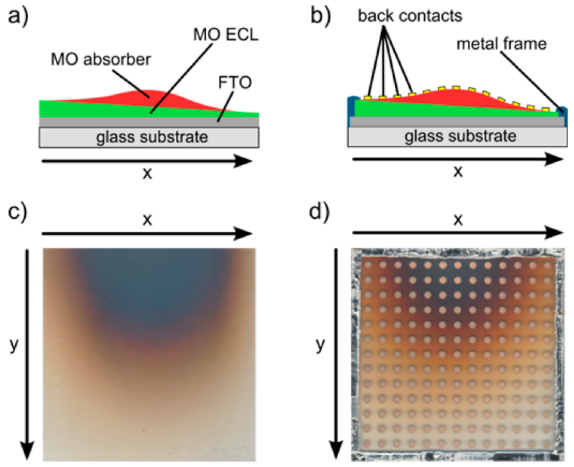

Figure 7. Combinatorial PV libraries. (a) Schematic drawing of a combinatorial device library cross section showing the linear TiO_2 gradient and the bell-shaped CuO profile before deposition of the BCs. (b) Like (a) including BC patches and the soldered frame that connects to the FTO layer. (c) Photograph of the TiO_2/CuO device library used for optical measurements before deposition of the contacts. (d) Photograph of a combinatorial thin film PV device library with a grid of 13 × 13 BCs.

Automated scanning characterization systems were developed to analyze the optical transmission and reflection as well as the $I-V$ characteristics in the dark and under illumination. A map of the optical density αd measured at 700 nm is shown in Figure 8a, recorded with an $x-y$ scanning stage in conjunction with fiber-optics-coupled CCD array spectrophotometers and two integrating spheres to include scattering for total transmission and reflection. $I-V$ scans were performed on each point using an automated $x-y-z$ scanning system. A spring-loaded Au-coated metal tip was automatically brought to the metal patch making temporary electrical contact for each individual measurement, while a metal clip provided permanent electrical contact via the soldered frame to the joint FTO FC. $I-V$ scans were performed in the dark and under illumination, where a Xe lamp with an AM1.5G filter was used to provide a spectrum in good agreement with sunlight (100 mW/cm^2). The light was coupled through optical fibers to the scanning system illuminating only a single cell during $I-V$ characterization of the entire library. It should be noted that the small patch size of ~4 mm^2 can lead to a systematic error of the current density J_{sc} due to edge effects. Consequently, current densities recorded on a single library can be compared with each other, but for comparison with literature values, measurement errors due to the small cell size might exist. Maps of the J_{sc}, V_{oc}, and the maximum power P_{max} (100 $\mu W/cm^2$ corresponds to a conversion efficiency η of 0.1%) are shown in Figure 8b–d. It can be seen that the highest currents were achieved with semitransparent cells that are located at the periphery of the CuO deposition with low optical density, illustrating a mismatch between light penetration and the minority carrier diffusion length, $L_D \ll \alpha^{-1}$. This example demonstrates the power of combinatorial methods where a violation of criteria (vi) for efficient PV device operation is revealed by a single library. Moreover, the horizontal asymmetries in the parameter maps of Figure 8 indicate that this cell performs better when the electron-conducting layer (TiO_2) is thin (right-hand side). These device combinatorial concepts significantly improve the ability to develop and

dx.doi.org/10.1021/jz3017039 | J. Phys. Chem. Lett. 2012, 3, 3755–3764

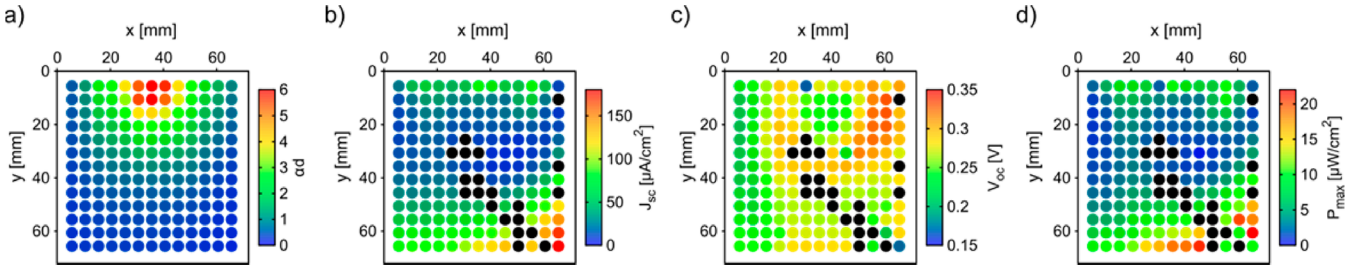

Figure 8. (a) Map of the optical density αd at 700 nm measured on the sample shown in Figure 7a,c. (b) J_{sc} map for the library shown in (a), with black dots indicating that these cells did not show PV performance. (c) V_{oc} and (d) maximum power density P_{max} maps of the all-oxide PV library shown in Figure 7b,d.

understand new MO absorbers as described in the following section.

Combinatorial PV Material Development. The all-oxide PV cells presented above are a promising start for the search of oxide semiconductors for PVs, but the photovoltage and especially the photocurrent still leave much room for improvement. Efficient all-oxide PV cells require the development of novel MO semiconductors with the desired optical and electronic properties such as high minority carrier mobilities, a suitable band gap between 0.9 and 1.7 eV for single-junction cells, suitable work function and energy levels of the band edges, and a strong optical absorption coefficient. The prospect of finding these unique materials lies in combinatorial material science, which can produce novel MOs consisting of two, three, four, or more elements. While most binary MOs are known, the number of unknown compositions drastically increases with the number of components, $A_kB_lO_n$, $A_kB_lC_mO_n$, and so forth, with A, B, and C being different metals and k, l, m, and n being integers. The most prominent example where the increase of the number of elements in the studied materials resulted in significant performance improvement relates to the development of high-temperature superconductors,[83] shown in Figure 9. Over the years, the critical temperature (where the material is

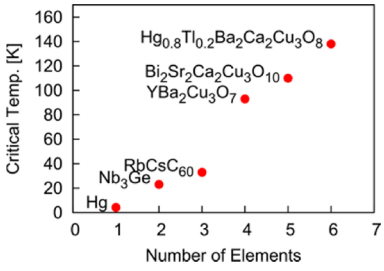

Figure 9. Increasing transition temperature of superconductors with increasing material complexity.

losing its superconducting properties) was successfully increased from a few Kelvin for Hg up to almost 140 K, synthesizing a material that consists of six different elements. Figure 9 shows that with increasing complexity of the material, outstanding electronic properties were found. It should furthermore be noticed that the superconductors with the highest critical temperatures are all metal oxides.

Combinatorial MO synthesis allows production of a large number of material compositions on a single substrate. In conjunction with large-throughput characterization methods, fast progress for the development of new materials is in reach.[84] Combinatorial methods have been used to develop transparent conducting oxides,[85] luminescent materials,[86] new semiconductors,[87] thermoelastic shape memory alloys,[88] photoelectrodes for solar water splitting,[89,90] and organic[91] and inorganic thin films PVs.[92] Continuous compositional spreads take advantage of the inhomogeneous thickness profile of a deposition process such as sputtering or PLD. The principle is shown in Figure 10 for PLD for a combinatorial MO deposition

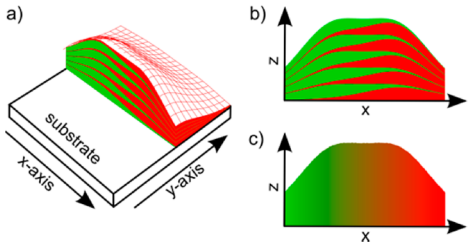

Figure 10. Combinatorial material synthesis for novel MOs. (a) Three-dimensional illustration with the cross section of a combinatorial deposition carried out by PLD using two known MOs (shown in red and green). (b) Schematic cross section along the center of the deposition profiles. (c) Thermal treatment leads to a complete intermixture of the layered structure with a lateral compositional gradient.

composed of two metal oxides (red and green). Sample movement in conjunction with target exchange enables the deposition of two or three different materials consecutively with their deposition maximum in different locations on the substrate. Thin films can be built up by repeating the deposition cycle hundreds of times, where a small number of laser pulses per cycle guarantees the deposition of thin layers with a maximum thickness on the order of the crystal unit cell of the pure material. Figure 10a,b shows the layered structure of a binary material produced by PLD, which can be converted by heat treatment into a film with a homogeneous composition along the z-direction while its composition changes as a function of the lateral coordinates (Figure 10c). In this way, it is possible to produce materials in a single deposition process with a composition ranging from doping of MO1 with MO2, an intermixing regime with all possible ratios of MO1 and MO2, to doping of MO2 with MO1.

The new materials are tested in combinatorial PV device libraries as presented above to investigate them under PV operating conditions. Data storage and data handling are organized using a database, and tools for data mining known from fields of combinatorial biology, chemistry, or drug development are applied to reveal unexpected or complex correlations between the material properties and the device performance and to improve our understanding of all-oxide PV device operation.

dx.doi.org/10.1021/jz3017039 | J. Phys. Chem. Lett. 2012, 3, 3755−3764

With nearly unlimited possible metal oxide compositions, studies in these directions are expected to significantly impact both basic and applied PV research.

Outlook. All-oxide PV cells are promising to realize extremely cheap PV systems. So far, all-oxide PV cells with a Cu_2O, CuO, Co_3O_4, Fe_2O_3, and $BiFeO_3$ absorber have been realized. While promising conversion efficiencies are reported for the Cu_2O system, low conversion efficiencies are achieved with the other MO absorbers. With new MOs, we expect to realize thin film PV cells with comparable performance to existing thin film technologies but at an extremely reduced fabrication cost. Combinatorial synthesis, large-throughput characterization, and computational data analysis methods have proven to be very effective in other areas of research and development, ranging from the pharmaceutical industry, biology and chemistry, to solid-state physics. Transferring the concept to the development of new PV materials is a powerful approach that enables production of a large number of materials in a short time, characterization of them, and definition of the directions of progress. With nearly unlimited possible MO compositions, studies in these directions are expected to significantly impact both basic and applied PV research.

AUTHOR INFORMATION

Corresponding Author

*E-mail: sven.ruhle@gmail.com (S.R.); Arie.Zaban@biu.ac.il (A.Z.).

Author Contributions

The manuscript was written through contributions of all authors. All authors have given approval to the final version of the manuscript.

Funding

The authors acknowledge financial support from the Israeli National Nanotechnology Initiative (INNI, FTA project) and from the Kamin project.

Notes

The authors declare no competing financial interest.

Biographies

Sven Rühle received his Ph.D. from the Weizmann Institute of Science (Rehovot, Israel) where he worked on extreme thin absorber and dye-sensitized solar cells. As a postdoc, he investigated ZnO nanowire luminescence and lasing at the Debye Institute (Utrecht University, The Netherlands). Back in Israel, he joined the Zaban group, where he is currently the head of the "Combinatorial Material Science for All-Oxide Photovoltaics" project. http://www.zabanlab.com

Assaf Anderson received his Ph.D. degree from the Imperial College London (United Kingdom), majoring in photochemistry and nano devices. He received his B.Sc. & M.Sc. degrees from Bar Ilan University, majoring in materials science and nanotechnology. After his Ph.D., he returned to Bar Ilan University as a research fellow.

Hannah-Noa Barad has conducted the research for her master thesis within the "Combinatorial Material Science for All-Oxide Photovoltaics" project, focusing on CuO and Cu_2O light absorbers.

Benjamin Kupfer received his B.Sc. from the Technion (Haifa, Israel) and his M.Sc. from the University College of London (United Kingdom). His Ph.D. research is focused on the investigation of all-oxide PV cells based on Co_3O_4 absorbers.

Yaniv Bouhadana received his Ph.D. from Bar Ilan University, where he investigated methods for water desalination using electrochemical means. As a postdoc, he joined the "Combinatorial Material Science for All-Oxide Photovoltaics" project, where he is developing computational tools for large-throughput material characterization and data management.

Eli Rosh-Hodesh has worked for many years in the Israeli high tech industry, where he has gained his expertise in materials research and development. Currently, he is developing low-cost processes for metal oxide synthesis.

Arie Zaban earned a B.Sc. in Chemistry and a Ph.D. in Electrochemistry from Bar Ilan University. After a 2 year postdoctoral stint at the U.S. National Renewable Energy Laboratory (Denver, CO), he was appointed to the senior faculty at Bar Ilan, where he is currently a Full Professor of Chemistry and Director of the Bar Ilan Institute for Nanotechnology and Advanced Materials. http://www.zabanlab.com

REFERENCES

(1) Jäger-Waldau, A. Thin Film Photovoltaics: Markets and Industry. *Int. J. Photoenergy* **2012**, *2012*, 768368.

(2) Masson, G.; Latour, M.; Biancardi, D. *Global Market Outlook for Photovoltaics Until 2016*; European Photovoltaic Industry Association: Brussels, Belgium, 2012.

(3) Branker, K.; Pathak, M. J. M.; Pearce, J. M. A Review of Solar Photovoltaic Levelized Cost of Electricity. *Renewable. Sustainable Energy Rev.* **2011**, *15*, 4470−4482.

(4) Fortunato, E.; Ginley, D.; Hosono, H.; Paine, D. C. Transparent Conducting Oxides for Photovoltaics. *MRS Bull.* **2007**, *32*, 242−247.

(5) Ginley, D. S.; Bright, C. Transparent Conducting Oxides. *MRS Bull.* **2000**, *25*, 15−18.

(6) Fortunato, E.; Barquinha, P.; Martins, R. Oxide Semiconductor Thin-Film Transistors: A Review of Recent Advances. *Adv. Mater.* **2012**, *24*, 2945−2986.

(7) Hagfeldt, A. Brief Overview of Dye-Sensitized Solar Cells. *Ambio* **2012**, *41*, 151−155.

(8) Rühle, S.; Shalom, M.; Zaban, A. Quantum-Dot-Sensitized Solar Cells. *ChemPhysChem* **2010**, *11*, 2290−2304.

(9) Dittrich, T.; Belaidi, A.; Ennaoui, A. Concepts of Inorganic Solid-State Nanostructured Solar Cells. *Sol. Energy Mater. Sol. Cells* **2011**, *95*, 1527−1536.

(10) Jose, R.; Thavasi, V.; Ramakrishna, S. Metal Oxides for Dye-Sensitized Solar Cells. *J. Am. Ceram. Soc.* **2009**, *92*, 289−301.

(11) Guijarro, N.; Lutz, T.; Lana-Villarreal, T.; O'Mahony, F.; Gómez, R.; Haque, S. A. Toward Antimony Selenide Sensitized Solar Cells: Efficient Charge Photogeneration at spiro-OMeTAD/Sb_2Se_3/Metal Oxide Heterojunctions. *J. Phys. Chem. Lett.* **2012**, *3*, 1351−1356.

(12) Kamat, P. V. TiO_2 Nanostructures: Recent Physical Chemistry Advances. *J. Phys. Chem. C* **2012**, *116*, 11849−11851.

(13) Anta, J. A.; Guillén, E.; Tena-Zaera, R. ZnO-Based Dye-Sensitized Solar Cells. *J. Phys. Chem. C* **2012**, *116*, 11413−11425.

(14) Ferrere, S.; Zaban, A.; Gregg, B. A. Dye Sensitization of Nanocrystalline Tin Oxide by Perylene Derivatives. *J. Phys. Chem. B* **1997**, *101*, 4490−4493.

(15) Burnside, S.; Moser, J. E.; Brooks, K.; Grätzel, M.; Cahen, D. Nanocrystalline Mesoporous Strontium Titanate as Photoelectrode Material for Photosensitized Solar Devices: Increasing Photovoltage Through Flatband Potential Engineering. *J. Phys. Chem. B* **1999**, *103*, 9328−9332.

(16) Lenzmann, F.; Krueger, J.; Burnside, S.; Brooks, K.; Grätzel, M.; Gal, D.; Rühle, S.; Cahen, D. Surface Photovoltage Spectroscopy of Dye-Sensitized Solar Cells with TiO_2, Nb_2O_5, and $SrTiO_3$ Nanocrystalline Photoanodes: Indication for Electron Injection from Higher Excited Dye States. *J. Phys. Chem. B* **2001**, *105*, 6347−6352.

(17) Greenwald, S.; Rühle, S.; Shalom, M.; Yahav, S.; Zaban, A. Unpredicted Electron Injection in CdS/CdSe Quantum Dot Sensitized ZrO_2 Solar Cells. *Phys. Chem. Chem. Phys.* **2011**, *13*, 19302−19306.
(18) He, J.; Lindström, H.; Hagfeldt, A.; Lindquist, S.-E. Dye-Sensitized Nanostructured p-Type Nickel Oxide Film as a Photocathode for a Solar Cell. *J. Phys. Chem. B* **1999**, *103*, 8940−8943.
(19) Green, M. A.; Emery, K.; Hishikawa, Y.; Warta, W.; Dunlop, E. D. Solar Cell Efficiency Tables (Version 40). *Prog. Photovoltaics* **2012**, *20*, 606−614.
(20) Yella, A.; Lee, H.-W.; Tsao, H. N.; Yi, C.; Chandiran, A. K.; Nazeeruddin, M. K.; Diau, E. W.-G.; Yeh, C.-Y.; Zakeeruddin, S. M.; Grätzel, M. Porphyrin-Sensitized Solar Cells with Cobalt (II/III)-Based Redox Electrolyte Exceed 12% Efficiency. *Science* **2011**, *334*, 629−634.
(21) Lee, M. M.; Teuscher, J.; Miyasaka, T.; Murakami, T. N.; Snaith, H. J. Efficient Hybrid Solar Cells Based on Meso-Superstructured Organometal Halide Perovskites. *Science* **2012**, *338*, 643−647.
(22) O'Regan, B. C.; Durrant, J. R.; Sommeling, P. M.; Bakker, N. J. Influence of the $TiCl_4$ Treatment on Nanocrystalline TiO_2 Films in Dye-Sensitized Solar Cells. 2. Charge Density, Band Edge Shifts, and Quantification of Recombination Losses at Short Circuit. *J. Phys. Chem. C* **2007**, *111*, 14001−14010.
(23) Krunks, M.; Dedova, T.; Oja Açik, I. Spray Pyrolysis Deposition of Zinc Oxide Nanostructured Layers. *Thin Solid Films* **2006**, *515*, 1157−1160.
(24) Law, M.; Greene, L. E.; Johnson, J. C.; Saykally, R.; Yang, P. Nanowire Dye-Sensitized Solar Cells. *Nat. Mater.* **2005**, *4*, 455−459.
(25) Elias, J.; Tena-Zaera, R.; Wang, G.-Y.; Lévy-Clément, C. Conversion of ZnO Nanowires into Nanotubes with Tailored Dimensions. *Chem. Mater.* **2008**, *20*, 6633−6637.
(26) Gao, P. X.; Ding, Y.; Mai, W.; Hughes, W. L.; Lao, C.; Wang, Z. L. Conversion of Zinc Oxide Nanobelts into Superlattice-Structured Nanohelices. *Science* **2005**, *309*, 1700−1704.
(27) Shen, G.; Bando, Y.; Chen, D.; Liu, B.; Zhi, C.; Golberg, D. Morphology-Controlled Synthesis of ZnO Nanostructures by a Simple Round-to-Round Metal Vapor Deposition Route. *J. Phys. Chem. B* **2006**, *110*, 3973−3978.
(28) Klingshirn, C. ZnO: From Basics Towards Applications. *Phys. Status Solidi B* **2007**, *244*, 3027−3073.
(29) Arango, A. C.; Johnson, L. R.; Bliznyuk, V. N.; Schlesinger, Z.; Carter, S. A.; Hörhold, H. H. Efficient Titanium Oxide/Conjugated Polymer Photovoltaics for Solar Energy Conversion. *Adv. Mater.* **2000**, *12*, 1689−1692.
(30) Ravirajan, P.; Peiro, A. M.; Nazeeruddin, M. K.; Grätzel, M.; Bradley, D. D. C.; Durrant, J. R.; Nelson, J. Hybrid Polymer/Zinc Oxide Photovoltaic Devices with Vertically Oriented ZnO Nanorods and an Amphiphilic Molecular Interface Layer. *J. Phys. Chem. B* **2006**, *110*, 7635−7639.
(31) Boucle, J.; Ravirajan, P.; Nelson, J. Hybrid Polymer−Metal Oxide Thin Films for Photovoltaic Applications. *J. Mater. Chem.* **2007**, *17*, 3141−3153.
(32) Atienzar, P.; Ishwara, T.; Illy, B. N.; Ryan, M. P.; O'Regan, B. C.; Durrant, J. R.; Nelson, J. Control of Photocurrent Generation in Polymer/ZnO Nanorod Solar Cells by Using a Solution-Processed TiO_2 Overlayer. *J. Phys. Chem. Lett.* **2010**, *1*, 708−713.
(33) Steirer, K. X.; Chesin, J. P.; Widjonarko, N. E.; Berry, J. J.; Miedaner, A.; Ginley, D. S.; Olson, D. C. Solution Deposited NiO Thin-Films as Hole Transport Layers in Organic Photovoltaics. *Org. Electron.* **2010**, *11*, 1414−1418.
(34) Espinosa, N.; Dam, H. F.; Tanenbaum, D. M.; Andreasen, J. W.; Jørgensen, M.; Krebs, F. C. Roll-to-Roll Processing of Inverted Polymer Solar Cells using Hydrated Vanadium(V) Oxide as a PEDOT:PSS Replacement. *Materials* **2011**, *4*, 169−182.
(35) Li, F.; Ruan, S.; Xu, Y.; Meng, F.; Wang, J.; Chen, W.; Shen, L. Semitransparent Inverted Polymer Solar Cells Using MoO_3/Ag/WO_3 as Highly Transparent Anodes. *Sol. Energy Mater. Sol. Cells* **2011**, *95*, 877−880.
(36) Kim, D. Y.; Subbiah, J.; Sarasqueta, G.; So, F.; Ding, H.; Gao, Y. The Effect of Molybdenum Oxide Interlayer on Organic Photovoltaic Cells. *Appl. Phys. Lett.* **2009**, *95*, 093304/1−093304/3.
(37) Meyer, J.; Hamwi, S.; Kröger, M.; Kowalsky, W.; Riedl, T.; Kahn, A. Transition Metal Oxides for Organic Electronics: Energetics, Device Physics and Applications. *Adv. Mater.* **2012**, *24*, 5408−5427.
(38) Ratcliff, E. L.; Zacher, B.; Armstrong, N. R. Selective Interlayers and Contacts in Organic Photovoltaic Cells. *J. Phys. Chem. Lett.* **2011**, *2*, 1337−1350.
(39) Iwanowski, R. J.; Trivich, D. Enhancement of the Photovoltaic Conversion Efficiency in Cu/Cu_2O Schottky Barrier Solar Cells by H^+ Ion Irradiation. *Phys. Status Solidi A* **1986**, *95*, 735−741.
(40) Olsen, L.; Addis, F.; Miller, W. Experimental and Theoretical Studies of Cu_2O Solar Cells. *Sol. Cells* **1982**, *7*, 247−279.
(41) Olsen, L. C.; Bohara, R. C.; Urie, M. W. Explanation for Low-Efficiency Cu_2O Schottky-Barrier Solar Cells. *Appl. Phys. Lett.* **1979**, *34*, 47−49.
(42) Herion, J.; Niekisch, E. A.; Scharl, G. Investigation of Metal Oxide/Cuprous Oxide Heterojunction Solar Cells. *Sol. Energy Mater.* **1980**, *4*, 101−112.
(43) Jeong, S. S.; Mittiga, A.; Salza, E.; Masci, A.; Passerini, S. Electrodeposited ZnO/Cu_2O Heterojunction Solar Cells. *Electrochim. Acta* **2008**, *53*, 2226−2231.
(44) Katayama, J.; Ito, K.; Matsuoka, M.; Tamaki, J. Performance of Cu_2O/ZnO Solar Cell Prepared by Two-Step Electrodeposition. *J. Appl. Electrochem.* **2004**, *34*, 687−692.
(45) Mittiga, A.; Salza, E.; Sarto, F.; Tucci, M.; Vasanthi, R. Heterojunction Solar Cell with 2% Efficiency Based on a Cu_2O substrate. *Appl. Phys. Lett.* **2006**, *88*, 163502/1−163502/2.
(46) Minami, T.; Nishi, Y.; Miyata, T.; Nomoto, J.-i. High-Efficiency Oxide Solar Cells with ZnO/Cu_2O Heterojunction Fabricated on Thermally Oxidized Cu_2O Sheets. *Appl. Phys. Exp.* **2011**, *4*, 062301.
(47) Nishi, Y.; Miyata, T.; Minami, T. Effect of Inserting a Thin Buffer Layer on the Efficiency in n-ZnO/p-Cu_2O Heterojunction Solar Cells. *J. Vac. Sci. Technol., A* **2012**, *30*, 04D103−04D106.
(48) Han, K.; Tao, M. Electrochemically Deposited p−n Homojunction Cuprous Oxide Solar Cells. *Sol. Energy Mater. Sol. Cells* **2009**, *93*, 153−157.
(49) McShane, C. M.; Choi, K.-S. Junction Studies on Electrochemically Fabricated p−n Cu_2O Homojunction Solar Cells for Efficiency Enhancement. *Phys. Chem. Chem. Phys.* **2012**, *14*, 6112−6118.
(50) McShane, C. M.; Siripala, W. P.; Choi, K.-S. Effect of Junction Morphology on the Performance of Polycrystalline Cu_2O Homojunction Solar Cells. *J. Phys. Chem. Lett.* **2010**, *1*, 2666−2670.
(51) Wei, H. M.; Gong, H. B.; Chen, L.; Zi, M.; Cao, B. Q. Photovoltaic Efficiency Enhancement of Cu_2O Solar Cells Achieved by Controlling Homojunction Orientation and Surface Microstructure. *J. Phys. Chem. C* **2012**, *116*, 10510−10515.
(52) Wijesundera, R. P. Fabrication of the CuO/Cu_2O Heterojunction Using an Electrodeposition Technique for Solar Cell Applications. *Semicond. Sci. Technol.* **2010**, *25*, 045015.
(53) Cui, J.; Gibson, U. J. A Simple Two-Step Electrodeposition of Cu_2O/ZnO Nanopillar Solar Cells. *J. Phys. Chem. C* **2010**, *114*, 6408−6412.
(54) Musselman, K. P.; Marin, A.; Schmidt-Mende, L.; MacManus-Driscoll, J. L. Incompatible Length Scales in Nanostructured Cu_2O Solar Cells. *Adv. Funct. Mater.* **2012**, *22*, 2202−2208.
(55) Musselman, K. P.; Marin, A.; Wisnet, A.; Scheu, C.; MacManus-Driscoll, J. L.; Schmidt-Mende, L. A Novel Buffering Technique for Aqueous Processing of Zinc Oxide Nanostructures and Interfaces, and Corresponding Improvement of Electrodeposited ZnO−Cu_2O Photovoltaics. *Adv. Funct. Mater.* **2011**, *21*, 573−582.
(56) Musselman, K. P.; Wisnet, A.; Iza, D. C.; Hesse, H. C.; Scheu, C.; MacManus-Driscoll, J. L.; Schmidt-Mende, L. Strong Efficiency Improvements in Ultra-Low-Cost Inorganic Nanowire Solar Cells. *Adv. Mater.* **2010**, *22*, E254−E258.
(57) Yuhas, B. D.; Yang, P. Nanowire-Based All-Oxide Solar Cells. *J. Am. Chem. Soc.* **2009**, *131*, 3756−3761.

(58) de Jongh, P. E.; Vanmaekelbergh, D.; Kelly, J. J. Cu_2O: Electrodeposition and Characterization. *Chem. Mater.* **1999**, *11*, 3512−3517.
(59) Li, D.; Chien, C.-J.; Deora, S.; Chang, P.-C.; Moulin, E.; Lu, J. G. Prototype of a Scalable Core−Shell Cu_2O/TiO_2 Solar Cell. *Chem. Phys. Lett.* **2011**, *501*, 446−450.
(60) Choi, T.; Lee, S.; Choi, Y. J.; Kiryukhin, V.; Cheong, S.-W. Switchable Ferroelectric Diode and Photovoltaic Effect in $BiFeO_3$. *Science* **2009**, *324*, 63−66.
(61) Seidel, J.; Fu, D.; Yang, S.-Y.; Alarcón-Lladó, E.; Wu, J.; Ramesh, R.; Ager, J. W., III. Efficient Photovoltaic Current Generation at Ferroelectric Domain Walls. *Phys. Rev. Lett.* **2011**, *107*, 126805.
(62) Yang, S. Y.; Martin, L. W.; Byrnes, S. J.; Conry, T. E.; Basu, S. R.; Paran, D.; Reichertz, L.; Ihlefeld, J.; Adamo, C.; Melville, A.; et al. Photovoltaic Effects in $BiFeO_3$. *Appl. Phys. Lett.* **2009**, *95*, 062909/1−062909/3.
(63) Yang, S. Y.; Seidel, J.; Byrnes, S. J.; Shafer, P.; Yang, C. H.; Rossell, M. D.; Yu, P.; Chu, Y. H.; Scott, J. F.; Ager, J. W.; et al. Above-Bandgap Voltages from Ferroelectric Photovoltaic Devices. *Nat. Nano.* **2010**, *5*, 143−147.
(64) Rai, B. P. Cu_2O Solar Cells: A Review. *Sol. Cells* **1988**, *25*, 265−272.
(65) Rakhshani, A. E. Preparation, Characteristics and Photovoltaic Properties of Cuprous Oxide — A Review. *Solid-State Electron.* **1986**, *29*, 7−17.
(66) Shockley, W.; Queisser, H. J. Detailed Balance Limit of Efficiency of p−n Junction Solar Cells. *J. Appl. Phys.* **1961**, *32*, 510−519.
(67) Brown, A. S.; Green, M. A. Detailed Balance Limit for the Series Constrained Two Terminal Tandem Solar Cell. *Physica E* **2002**, *14*, 96−100.
(68) Musa, A. O.; Akomolafe, T.; Carter, M. J. Production of Cuprous Oxide, a Solar Cell Material, by Thermal Oxidation and a Study of its Physical and Electrical Properties. *Sol. Energy Mater. Sol. Cells* **1998**, *51*, 305−316.
(69) Golden, T. D.; Shumsky, M. G.; Zhou, Y.; VanderWerf, R. A.; Van Leeuwen, R. A.; Switzer, J. A. Electrochemical Deposition of Copper(I) Oxide Films. *Chem. Mater.* **1996**, *8*, 2499−2504.
(70) Schwartz, D. T.; Muller, R. H. Oxidation Films on Copper in Alkaline Media: Intensity Modulated Photoelectrochemical and Raman Spectroscopy Studies. *Surf. Sci.* **1991**, *248*, 349−358.
(71) Kosugi, T.; Kaneko, S. Novel Spray-Pyrolysis Deposition of Cuprous Oxide Thin Films. *J. Am. Ceram. Soc.* **1998**, *81*, 3117−3124.
(72) Deuermeier, J.; Gassmann, J.; Brotz, J.; Klein, A. Reactive Magnetron Sputtering of Cu_2O: Dependence on Oxygen Pressure and Interface Formation with Indium Tin Oxide. *J. Appl. Phys.* **2011**, *109*, 113704−113707.
(73) Hameş, Y.; Eren San, S. CdO/Cu_2O Solar Cells by Chemical Deposition. *Solar Energy* **2004**, *77*, 291−294.
(74) Wang, L.; Tao, M. Fabrication and Characterization of p−n Homojunctions in Cuprous Oxide by Electrochemical Deposition. *Electrochem. Solid-State Lett.* **2007**, *10*, H248−H250.
(75) Scanlon, D. O.; Watson, G. W. Undoped n-Type Cu_2O: Fact or Fiction? *J. Phys. Chem. Lett.* **2010**, *1*, 2582−2585.
(76) Green, M. A. Photovoltaic Principles. *Physica E* **2002**, *14*, 11−17.
(77) Würfel, P. *Physics of Solar Cells — From Principles to New Concepts*; Wiley-VCH: New York, 2005.
(78) Jaegermann, W.; Klein, A.; Mayer, T. Interface Engineering of Inorganic Thin-Film Solar Cells — Materials-Science Challenges for Advanced Physical Concepts. *Adv. Mater.* **2009**, *21*, 4196−4206.
(79) Rühle, S.; Yahav, S.; Greenwald, S.; Zaban, A. Importance of Recombination at the TCO/Electrolyte Interface for High Efficiency Quantum Dot Sensitized Solar Cells. *J. Phys. Chem. C* **2012**, *116*, 17473−17478.
(80) Tauc, J.; Grigorovici, R.; Vancu, A. Optical Properties and Electronic Structure of Amorphous Germanium. *Phys. Status Solidi B* **1966**, *15*, 627−637.
(81) Caglar, Y.; Oral, D. D.; Caglar, M.; Ilican, S.; Thomas, M. A.; Wu, K.; Sun, Z.; Cui, J. Synthesis and Characterization of $(CuO)_x(ZnO)_{1-x}$ Composite Thin Films with Tunable Optical and Electrical Properties. *Thin Solid Films* **2012**, *520*, 6642−6647.
(82) Xu, Y.; Schoonen, M. A. A. The Absolute Energy Positions of Conduction and Valence Bands of Selected Semiconducting Minerals. *Am. Mineral.* **2000**, *85*, 543−556.
(83) Takeuchi, I. MRS Fall Meeting, Tutorial UU, Boston, 2011.
(84) Potyrailo, R.; Rajan, K.; Stoewe, K.; Takeuchi, I.; Chisholm, B.; Lam, H. Combinatorial and High-Throughput Screening of Materials Libraries: Review of State of the Art. *ACS Comb. Sci.* **2011**, *13*, 579−633.
(85) Perkins, J. D.; del Cueto, J. A.; Alleman, J. L.; Warmsingh, C.; Keyes, B. M.; Gedvilas, L. M.; Parilla, P. A.; To, B.; Readey, D. W.; Ginley, D. S. Combinatorial Studies of Zn−Al−O and Zn−Sn−O Transparent Conducting Oxide Thin Films. *Thin Solid Films* **2002**, *411*, 152−160.
(86) Danielson, E.; Golden, J. H.; McFarland, E. W.; Reaves, C. M.; Weinberg, W. H.; Di Wu, X. A Combinatorial Approach to the Discovery and Optimization of Luminescent Materials. *Nature* **1997**, *389*, 944−948.
(87) Mao, S. S. High Throughput Combinatorial Screening of Semiconductor Materials. *Appl. Phys. A: Mater. Sci. Process.* **2011**, *105*, 283−288.
(88) Cui, J.; Chu, Y. S.; Famodu, O. O.; Furuya, Y.; Hattrick-Simpers, J.; James, R. D.; Ludwig, A.; Thienhaus, S.; Wuttig, M.; Zhang, Z.; et al. Combinatorial Search of Thermoelastic Shape-Memory Alloys with Extremely Small Hysteresis Width. *Nat. Mater.* **2006**, *5*, 286−290.
(89) Stepanovich, A.; Sliozberg, K.; Schuhmann, W.; Ludwig, A. Combinatorial Development of Nanoporous WO_3 Thin Film Photoelectrodes for Solar Water Splitting by Dealloying of Binary Alloys. *Int. J. Hydrogen Energy* **2012**, *37*, 11618−11624.
(90) Jaramillo, T. F.; Baeck, S.-H.; Kleiman-Shwarsctein, A.; Choi, K.-S.; Stucky, G. D.; McFarland, E. W. Automated Electrochemical Synthesis and Photoelectrochemical Characterization of $Zn_{1-x}Co_xO$ Thin Films for Solar Hydrogen Production. *J. Comb. Chem.* **2005**, *7*, 264−267.
(91) Teichler, A.; Eckardt, R.; Hoeppener, S.; Friebe, C.; Perelaer, J.; Senes, A.; Morana, M.; Brabec, C. J.; Schubert, U. S. Combinatorial Screening of Polymer:Fullerene Blends for Organic Solar Cells by Inkjet Printing. *Adv. Energy Mater.* **2011**, *1*, 105−114.
(92) Kafizas, A.; Parkin, I. P. Inorganic Thin-Film Combinatorial Studies for Rapidly Optimising Functional Properties. *Chem. Soc. Rev.* **2012**, *41*, 738−781.